CrossMark

Experimental investigation of a water/nanofluid jacket performance in stack heat recovery

Houman Moradi Dalvand[1] · Ali Jabari Moghadam[1]

Abstract

The effects of nanofluids (Al_2O_3–water) on the overall thermal performance of an annular enclosure (or jacket) are experimentally investigated which is used for recovering waste heat from a typical stack of a gas heater. In the initial stages of the heating process, the inner cylindrical wall becomes hotter, while the bulk fluid is nearly at the preceding uniform temperature; hence, the wall heat flux is strongly enhanced at the beginning. Afterward a decline in the wall heat flux is observed due to increasing Rayleigh number and correspondingly generating cellular flows in the annulus that leads to temperature enhancement of the liquid. Using nanofluids has the advantage of improving key parameters such as Nusselt number. Nanofluids with higher nanoparticle concentrations need less response time to react to any changes in thermal environment, and consequently they have smaller time constant. Higher convective heat transfer coefficient as well as greater temperature uniformity in the enclosure is achieved by selecting nanofluids with larger values of nanoparticle concentration. The results also reveal that convective heat transfer coefficient and Nusselt number of nanofluids are comparatively enhanced with time, since hotter base fluid results in higher effective thermal conductivity.

Keywords Heat transfer enhancement · Nanofluid · Waste heat recovery · Annular enclosure · Thermal performance

List of symbols

A	Area (m²)
c_p	Specific heat (J kg⁻¹ K⁻¹)
D	Diameter (m)
h	Heat transfer coefficient (W m⁻² K⁻¹)
$\bar{h}$	Average heat transfer coefficient (W m⁻² K⁻¹)
k	Thermal conductivity (W m⁻¹ K⁻¹)
M	Mass (kg)
$\dot{m}$	Mass flow rate (kg s⁻¹)
Nu	Nusselt number
$\overline{Nu}$	Average Nusselt number
Q	Heat (J)
q	Heat transfer rate (W)
q''	Heat flux (W m⁻²)
$\bar{q}''$	Average heat flux (W m⁻²)
Ra	Rayleigh number
T	Temperature (°C)
$\overline{T}$	Average temperature (°C)
V	Volume (m³)
X	Temperature ratio
Y	Mass ratio
$\bar{v}$	Average velocity (m s⁻¹)

Greek symbols

ζ	Heat loss percentage
δ	Boundary layer thickness (m)
Δ	Conduction layer thickness (m)
ϕ	Nanoparticles volume fraction
ρ	Density (kg m⁻³)
τ_t	Time constant (s)

Subscripts

bf	Base fluid
e	Equivalent
eff	Effective
g	Gas
i	Inlet
l	Liquid
m	Mean or average
nf	Nanofluid
np	Nanoparticle
o	Outlet

✉ Ali Jabari Moghadam
  jm.ali.project@gmail.com

1 Faculty of Mechanical Engineering, Shahrood University of Technology, P.O. Box 316, Shahrood, Iran

S   Surface
t   Time (min)
vol Volume concentration

Introduction

Global warming is one of the most important burning issues of today's world. It occurs by human activities and increase in fossil fuels consumption. Due to these actions, the Earth atmosphere temperature is averagely increased day to day. Global warming also has the potential to change rainfall and snow patterns, increase droughts and severe storms. Nowadays, scientists and engineers around the world are working to improve the technology of renewable energy sources and recoverable energies to increase the amount of energy they produce and decrease their impact on the environment. Exhaust fumes are known as waste products, but these sources are substantially valuable for providing heat such as hot water for many different applications and reducing the necessity to burn fossil fuels more. One of the important ways to absorb more heat from the exhaust is to modify heat characteristics of the working fluid.

Nanofluids are suspensions of metallic or nonmetallic nanoparticles in a base fluid; this term was introduced by Choi [1]. A considerable increase in liquid thermal conductivity, heat transfer coefficient, and liquid viscosity are the unique characteristics of nanofluids. According to the importance of nanofluids thermophysical properties, different researches have been accomplished by scientists. Ghadimi et al. [2] performed theoretical and experimental investigations to measure some of these features. There is no doubt that producing a stable nanofluid can assist researchers to achieve correct results. Hwang et al. [3] explained two ways for production and dispersion of nanoparticles in nanofluids. It is evident that liquids have lower thermal conductivity than those of metals in solid phase [4]. For instance, the thermal conductivity of copper at room temperature is about 700 times greater than that of water and about 3000 times greater than that of engine oil. Also, metallic fluids possess much greater thermal conductivity, in contrast to nonmetallic media. Thus, fluids containing suspended metal particles are expected apparent enhanced thermal conductivities rather than pure fluids [5].

Masuda et al. [6] dispersed oxide nanoparticles (Al_2O_3 and TiO_2 with 4.3 mass%) in liquid and illustrated that the thermal conductivity is increased by 32 and 11%, respectively. Sridhara and Satapathy [7] studied the recent progresses on the physical and thermophysical characteristics of water/Al_2O_3 nanofluids. They reported that the improvement in the thermal conductivity is 2–36% by

adding a certain amount of Al_2O_3 nanoparticles into the working fluid. Grimm [8] dispersed aluminum particles (1–80 nm) in a fluid and claimed a 100% increase in the thermal conductivity of fluid for 0.5–10 mass%. Esfe et al. [9] evaluated the thermal conductivity of Al_2O_3/water nanofluids in a temperature range between 26 and 55 °C with the solid volume fraction up to 0.05. They found that the sensitivity of thermal conductivity to particle loading is increased by rising the temperature. When the nanofluids are served in condensing and evaporating systems, the nanoparticle deposition and nanoparticle suspension are two important parameters in nanofluids and they should be considered due to their effects on the efficiency of thermal systems [10]. Hung et al. [11] assessed a thermal management system using alumina (Al_2O_3)/water as the nanofluid for green power sources. They pointed out that the efficiency factor ratios were optimal at low flow rates and low concentrations. Values of R_{EF} were all below 1.0 at high flow rates. Amani et al. [12] showed that by rising the nanofluid temperature at high rates, the thermal conductivity of $MnFe_2O_4$/water increases in the absence of magnetic field, while it declines when the magnetic field is exerted. The maximum thermal conductivity enhancement is experienced 36.5 at 3% volume concentration of nanoparticles and under 400-g magnetic field.

Togun et al. [13] investigated the influence of eccentricity in both horizontal and vertical directions on heat transfer rate for various positions of annular passages. They presented different techniques, which are based on experimental and numerical investigations to enhance the thermal efficiency of heat exchanging equipment transport energy. Ravnik and Škerget [14] assessed a numerical method and present results of simulations of flow and heat transfer of nanofluids. They considered steady laminar regime of Al_2O_3, Cu and TiO_2 nanofluids with different Rayleigh number values. The highest heat transfer gain is concluded in the conduction dominated flow regime. Amani et al. [15] evaluated thermal conductivity of $MnFe_2O_4$ in the attendance of magnetic field by using ANN and genetic algorithm. They proved the usefulness of the developed ANN for the prediction of thermophysical properties of nanofluids. Arani et al. [16] investigated the natural convection heat and mass transfer characteristics in a square enclosure using water/Al_2O_3 nanofluid. They experienced that the average Nusselt number increases by adding the nanoparticles, while average Sherwood number declines. Abu-Nada et al. [17] represented that low aspect ratios are more beneficial in comparison with nanoparticles thermal conductivity at low Raleigh numbers in enclosures. They observed that increasing the volume fraction of nanoparticles above 5% declines the average Nusselt number of both Al_2O_3–water and CuO–water nanofluids at high Rayleigh numbers.

Amani et al. [18] structured different soft optimizing and computing methods such as ANN, empirical correlations and genetic algorithm to investigate the thermophysical properties of MWCNTs nanofluid. They observed that the ANN model is a more exact method to anticipate the thermal conductivity and viscosity of MNCNT/water nanofluid. Using the exhaust fumes has been observed to a few recent studies. Esfe et al. [19] studied the effect of using Fe/ethylene glycol nanofluids on the efficiency of energy devices. They found that the nanoparticles with the average size of 40 and 70 nm provide a significant efficiency at low concentration, respectively. Parizad et al. [20] investigated free convection of TiO_2–water nanofluid over the vertical and horizontal flat plates with steady heat flux by using PIV method. They revealed that the maximum reduction in the vertical velocity component at particle concentrations ($\phi = 0.1$) is in the vicinity of 4 and 3.3% for $q'' = 3000$ and 7000 w m^{-2}, respectively. Amani et al. [21] investigated the performance of ferrofluids in a metal foam tube under the magnetic field. They observed that the Nusselt number of Fe_3O_4/water at $Re = 200$ with $\phi = 2$ mass% increases by 36.2% under the low fluctuating magnetic field. Rashidi et al. [22] studied the concurrent use of nanofluids and inserts to increase heat transfer in energy conversion systems. They concluded that employing both of the nanofluid and inserts brings a significant improvement in heat transfer in comparison with using one of them solely. Moghadam et al. [23] investigated the effect of CuO water nanofluid on the thermal performance enhancement of a solar collector. They observed that using CuO water nanofluid increases solar efficiency by 16.7%. Ghadiri et al. [24] examined the effects of ferrofluids as a coolant to improve the efficiency of a PVT system. They expressed that by using a 3 mass% ferrofluid under an alternating magnetic field, the overall efficiency of the system can be improved by 45 and 50%. Moshizi et al. [25] studied mixed convection of Al_2O_3 nanofluids inside a vertical microannulus, considering various form of nanoparticle migration. They indicated that both the temperature-dependent and concentration-dependent buoyancy forces play an important role on nanoparticle migration and flow field. Javadi et al. [26] investigated the combined effects of incidence angle and nanofluid on heat transfer enhancement around a square obstacle. In their numerical study, a two-dimensional incompressible unsteady laminar flow of Al_2O_3–water nanofluid was considered around a hotter obstacle. An increase in Nu number was observed due to an increased nanoparticle concentration. Raei et al. [27] carried out an experimental investigation on the effects of using Al_2O_3/water nanofluids on the efficiency of double tube heat exchanger. According to the results, the transfer coefficient and fraction factor of nanofluid are increased by 23 and 25%,

respectively, at 0.15 vol% of γ-Al_2O_3. Shirejini et al. [28] presented the simulation of Al_2O_3–water nanofluid flow and forced convection around a rotating cylinder. They observed that the enhancement of the heat transfer rate is in the vicinity of 10.3% at $Re = 100$ and $\phi = 0.05$.

Shahriari et al. [29] studied the laminar convection heat transfer in an enclosure equipped by uniform sinusoidal roughness elements and filled by Al_2O_3 nanofluid. They observed that the Nusselt number is enhanced by increasing volume fraction of nanoparticles, with the significant effect at $\phi = 0.04$ for $Ra = 10^3$. Terhan and Comakli [30] designed a flue gas condenser to recover latent heat from exhaust flue gas. Over this study, annual fuel saving was announced as $ 407,396.16 by their economic analysis method. Shelke and Gohel [31] studied thermosyphon heat pipe technology for the increasing of fresh air temperature by using recovered exhaust heat. They used 50% BN + 50% Zn0 to increase the performance of heat pipe heat exchanger with increase in source temperature.

To the author's knowledge, there is no similar work in the literature to examine the effects of nanofluids on thermal characteristics of annular enclosures which serve as heat recovery media of stacks. There is actually little work on the effect of using particular nanofluids as an absorbing medium (the working fluid) on the performance of liquid enclosures. Understanding the jacket thermal behavior is necessary in analyzing and designing an enclosure as an effective means of heat recovery as well as a covering that encloses an intermediate space through which a temperature-controlling fluid flows. The aim of the current study is to recover waste heat from exhaust flue gas in the natural gas-fired district heating systems by means of a liquid jacket (enclosure) which forms the outer shell of stacks. Motivated by the potential of nanoparticles in promoting thermal properties of liquids, we study here the effects of particular nanofluid, H_2O/Al_2O_3, in an enclosure surrounding a typical stack. Some quantities such as liquid and surface temperatures are directly measured in the jacket influenced by the presence of water/Al_2O_3 nanofluid to evaluate its thermal key parameters. Applications include storage of hot fluids, cooling closed systems such as microprocessors and electronic devices as well as transients in startup or shutdown of operating systems. Meanwhile warm liquid enclosures can be used as a heat spring in household and industrial expenditures whenever it is needed.

Experimental setup and method

Apparatus

An experimental setup was built to investigate the thermal performance of a liquid jacket by using different working fluids (water and Al_2O_3/water). Schematic view and the components of the test section are shown in Fig. 1. The enclosure consists of two concentric pipes. The outer pipe is made of polyethylene Teflon material having outer diameter, inner diameter and length of 80, 50 and 770 mm, respectively. The inner pipe is made of stainless steel (304 SS) with 25 mm inner diameter, 1 mm thickness and 800 mm length. The outlet of a gas heater with 3 kW
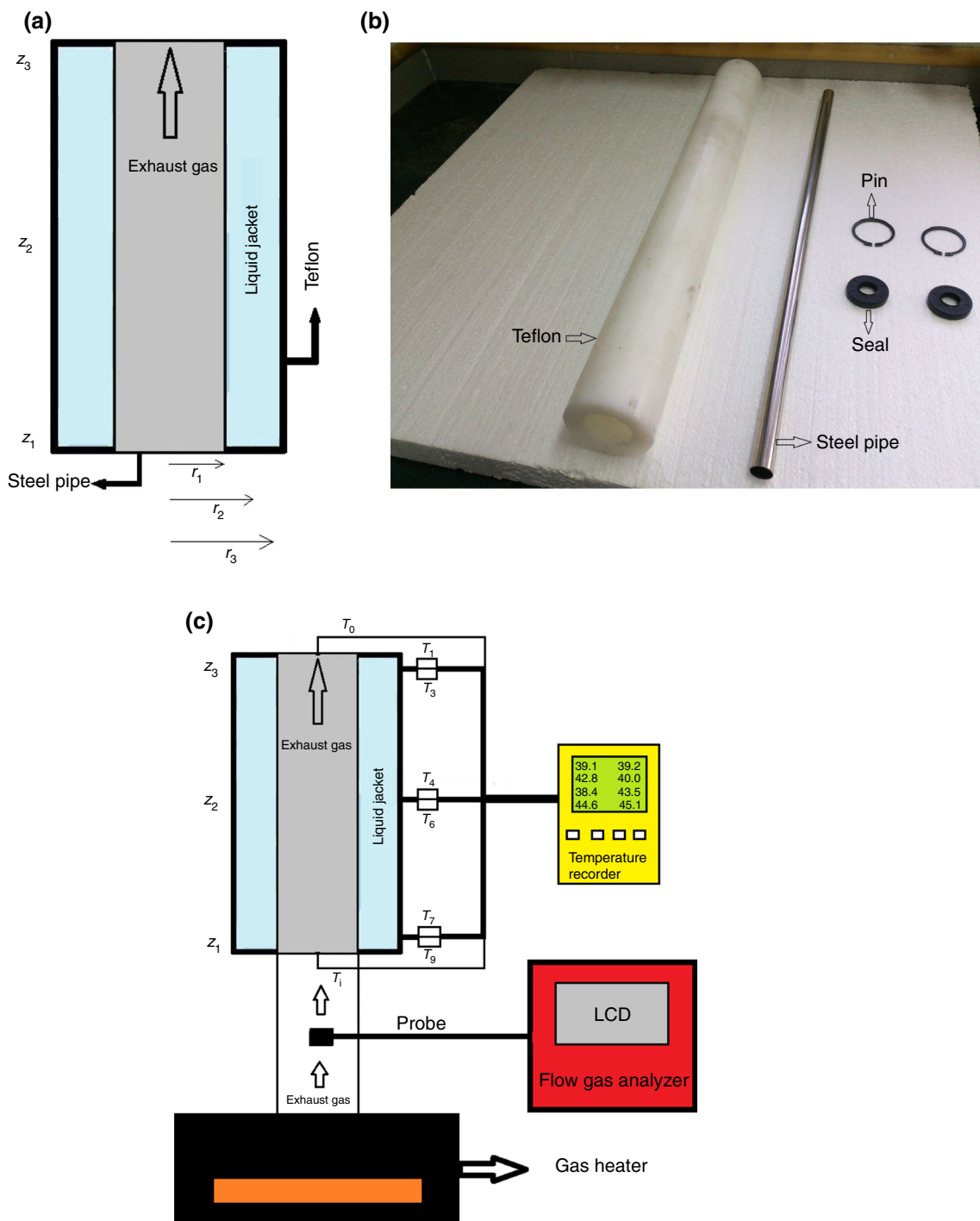

Fig. 1 a Schematic of the test section, **b** its components, and **c** schematic of the experimental setup

capacity is connected to the exhaust pipe (inner pipe), thereby heating gradually the working fluid around it. There are 12 k-type thermocouples with ± 0.01 °C error to measure working fluid temperatures at three different heights (z_1, z_2, z_3) and three different radii (r_1, r_2, r_3); exhaust gas temperatures at the inlet, middle and outlet of the inner pipe are also recorded. A 12-channel temperature recorder (Lutron BTM-4208SD) has been provided to obtain temperature values. A flow gas analyzer (Testo-350) has also been used to acquire density, specific heat, and average velocity of the exhaust gas listed in Table 1. The jacket was also insulated to minimize heat loss.

Nanofluid characterization and preparation

Water/Al_2O_3 nanofluids possess a noticeable potential in applications. Experimental and numerical data, related to the alumina-based nanofluids, have vividly illustrated that the augmentation of a certain amount of Al_2O_3 nanoparticle into pure water brings a significant increase in the thermal conductivity and heat transfer coefficients of the nanofluid. Nanofluids, Al_2O_3 in particular, are aimed to cool high heat flux devices and welding equipment as well as absorbing thermal energy. In this study, water and Al_2O_3 nanofluid were used as the working fluid. The aluminum oxide nanoparticles have average size and purity 15 nm and 99.5%, respectively; they are white and nearly spherical. Thermophysical properties of the nanoparticles are given in Table 2. In order to prepare a suitable and stable nanofluid with low or no agglomeration of nanoparticles, first certain amounts of Al_2O_3 nanoparticle were weighed by an electronic scale (accurate to 0.001 g) and then they were added to the distilled water as a base fluid. The suspensions were then homogenized by a high intensity ultrasonic system (Qsonica CL-334) generating ultrasonic pulses with a power of 300 W at 3 kHz. The suspensions were alternatively exposed to ultrasonic vibration for 2 h (Fig. 2). The volume fractions of nanoparticles in the fluids were 0.1 and 0.05%. It should be noted that no surfactant was used in alumina water suspensions because of the changes of their thermophysical characteristics. The thermophysical properties of the prepared nanofluids are calculated from nanoparticles and water characteristics. Pak and Cho [32] proposed the following equation to estimate the nanofluid density:

Table 1 Characteristics of the exhaust gas

Density/Kg m^{-3}	0.732
Heat capacity/J kg^{-1} K^{-1}	1024
Average velocity/m^{-1} s^{-1}	1.7

$$\rho_{nf} = (1 - \phi)\rho_{bf} + \phi\rho_{np} \tag{1}$$

where c_{pnf} is the effective specific heat of the nanofluid [33]:

$$c_{pnf} = \frac{\phi\rho_{np}c_{p,np} + (1 - \phi)\rho_{bf}c_{p,bf}}{(1 - \phi)\rho_{bf} + \phi\rho_{np}} \tag{2}$$

where ϕ indicates the volume friction of nanoparticles in a suspension of the base fluid. ρ is the density of material and subscripts f, np, and nf indicate fluid, nanoparticle, and nanofluid, respectively. Also, nanofluid effective thermal conductivity can be calculated by the following equation [34]:

$$\frac{k_{eff,nf}}{k_{bf}} = \frac{k_{np} + 2k_{bf} + 2\phi(k_{np} - k_{bf})}{k_{np} + 2k_{bf} - \phi(k_{np} - k_{bf})} \tag{3}$$

where k is the thermal conductivity and subscripts bf and np represent base fluid and nanoparticle, respectively.

Thermal analysis

The data of each test period are averaged and used in the analysis as a single point. The rate of heat transfer between the annulus inner wall and the jacket liquid is calculated by:

$$q = \bar{h}_t A_s (\bar{T}_s - \bar{T}_m) \tag{4}$$

in which, q is the rate of heat transfer, $\bar{h}_t$ is the average heat transfer coefficient, A_s is the heat transfer area, $\bar{T}_s$ and $\bar{T}_m$ are the average temperature of heat transfer surface and mean bulk temperature of the liquid (water or nanofluid), respectively. The temperature of the liquid rises where it is in contact with inner pipe surface. The exhaust gas, on the other hand, delivers a certain amount of thermal energy to the wall (between z_1 and z_3), which is ideally equal to the heat gained by the liquid:

$$q = \dot{m} c_{p,g}(T_i - T_o) \tag{5}$$

$$\dot{m} = \rho \bar{v} A \tag{6}$$

where q is the heat rate produced by the gas between two levels, $\dot{m}$ is the gas mass flow rate, $c_{p,g}$ is the gas specific heat; T_i and T_o are the gas inlet and outlet temperatures, respectively. It should be noted that density, specific heat, and velocity of the flue gas are measured by a flow gas analyzer measurement system. Equating the two previous equations, one can obtain the average convective heat transfer coefficient in the liquid jacket:
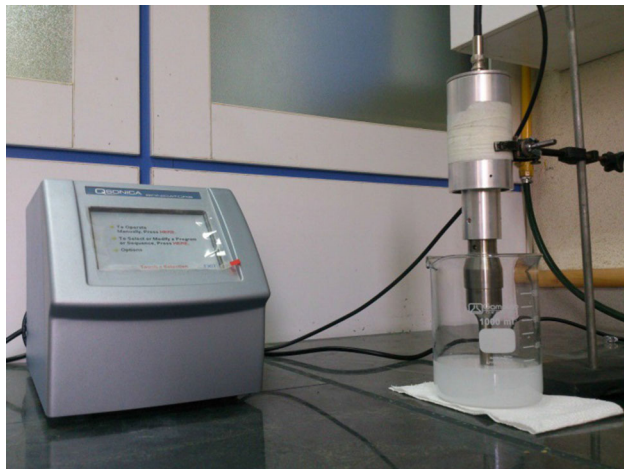
$$\bar{h}_t = \frac{\dot{m} c_{p,g}(T_i - T_o)}{A_s (\bar{T}_s - \bar{T}_m)} \tag{7}$$

Table 2 Some physical properties of water and γ-Al$_2$O$_3$ nanoparticle

Nanoparticle	Aluminum oxide/γ	Water (at 300 K)
Density/Kg^{-1} m^{-3}	3650	995.7
Specific heat/J Kg^{-1} K^{-1}	850	4180
Thermal conductivity/W^{-1} m^{-1} K^{-1}	42	0.62

Fig. 2 Preparation of the nanofluid

The average heat flux $\bar{q}_t''$ of the inner pipe can be expressed as:

$$\bar{q}_t'' = \bar{h}_t(\underbrace{\bar{T}_s - \bar{T}_m}_{\Delta\bar{T}_{s-m}}) \tag{8}$$

The average Nusselt number for water or nanofluid is then calculated by:

$$\bar{N}u_t = Nu = \frac{\bar{h}_t D_e}{k_{eff}} \tag{9}$$

in which k_{eff} is the effective thermal conductivity of liquid and D_e is the equivalent (characteristic) diameter of the liquid jacket (effective diameter of annulus area):

$$D_e = \frac{V}{A_s} \tag{10}$$

It is noted that V and A_s are the jacket volume and heat transfer surface, respectively.

The whole system is initially at room temperature. During the gas heater operation, thermal energy is continuously produced (Eq. 5) and transferred to the liquid:

$$Q_l = M_l\, c_{p,l}(\bar{T}_{m,t2} - \bar{T}_{m,t1}) \tag{11}$$

where Q_l is the heat required to increase the liquid temperature, $c_{p,l}$ is the liquid heat capacity, and $\Delta\bar{T}_{m,t} = \bar{T}_{m,t2} - \bar{T}_{m,t1}$ is the enhancement of the average bulk temperature of the liquid during a specific time interval. Considering the relation $Q_l = q.t$, we can obtain two dimensionless parameters:

$$X = \frac{\Delta\bar{T}_{m,t}}{(T_i - T_o)} \tag{12}$$

$$Y = \frac{\dot{m}\, c_{p,g}}{M_l c_{p,l}} \times t = \frac{t}{\tau_t} \tag{13}$$

where X is the temperature ratio and Y is the characteristic mass ratio. Also, τ_t is a time constant that indicates the relative ability of heat absorbing by fluids. In order to have a measure of heat loss in the liquid enclosure, the quantity ζ (heat loss percentage) is introduced as follows:

$$\zeta = \frac{\sum_{i=1}^{n}(X_i - Y_i)}{\sum_{i=1}^{n}X_i} \tag{14}$$

X and Y are calculated from Eqs. (12) and (13) and reported in the span of 4 min.

Assessment of time variations of the average temperature of the liquids reveals that the following analytic expression may be propounded:

$$\bar{T}_m = c_1 + c_2\exp\left(-\frac{c_3}{\tau_t}t\right) \tag{15}$$

in which, the coefficients c_1, c_2, and c_3 are given in Table 3.

Uncertainty analysis

Evaluation of errors in the experiments is necessary to carry out an authentic test. According to uncertainty analysis described by Moffat [35], uncertainty of experimental results is defined by measurement deflection of parameters such as mass flow rate, bulk fluid temperature and wall temperature. Thus, the error of each parameter is involved into the assessment of uncertainties. Average heat transfer coefficient is impressed by uncertainty of mass flow rate, heat transfer area, exhaust gas temperature, and average temperature of the heat transfer surface and the bulk fluid. Table 4 lists the accuracies and uncertainties of the measurements in the present study. It was calculated that maximum uncertainty in the measurement of the average heat transfer coefficient was 4.8% which is mostly related to the temperatures measurement.

Table 3 Coefficients of the mean temperature formula

	c_1	c_2	c_3	τ_t
Water	53.841428	− 31.841428	4.356046	8015.2
Nanofluid (0.05 vol%)	54.226428	− 32.226428	4.770697	8002.6
Nanofluid (0.1 vol%)	54.814577	− 32.814577	4.864496	7990.9

Table 4 Accuracy and uncertainty of the measured parameters

Quantity	Accuracy	Uncertainty/%
Fluid temperature	± 0.01 °C	0.09
Flow rate	± 1 mL	0.64
Time	± 0.01 s	0.08
Length	± 1 mm	0.02
Diameter	± 0.1 mm	0.0018

Results and discussion

In this study, two types of working fluids were employed: water and water/Al_2O_3 nanofluid with two different volume concentrations. For the sake of simplicity, these fluids are named as: liquid A (water); liquid B (water/Al_2O_3 nanofluid with 0.05% concentration); liquid C (water/Al_2O_3 nanofluid with 0.1% concentration). The time constant values (τ_t) for liquids A, B, and C are 8015.2, 8002.6 and 7990.9 s, respectively. It is noted that the liquid jacket is enclosed in the radial direction ($r_{31} = r_3 - r_1 = 12.5$ mm) with a thin-wall steel pipe (inner radius $= r_1$) and a thick-wall Teflon pipe (outer radius $= r_3$). Each experiment was performed in several days and the best experimental data, which have minimum errors and satisfy the standard conditions, have been selected.

Figure 3 shows variations in fluid temperature at three different r for the same level (z_2). It can be observed that increasing the temperature of working liquids with time follows a fairly similar pattern over the test period. From the beginning to the minute of 32, liquids A, B, and C experience temperature rises of 21.5, 23.3 and 24.5 °C, respectively, at r_1; then the rate of temperature rise decreases slightly. Maximum temperature enhancement is attained for liquid C (0.1% nanofluid) which is about 31.5 °C. The larger the value of concentration, the greater is the temperature difference between the inner and outer surfaces.

In Fig. 4, the fluid temperature varies with time at three different z for the same radius (r_2). The inner and outer walls of the enclosure are heated and cooled, respectively. Liquid motion is therefore characterized by a recirculating or cellular flow for which fluid ascends along the hot wall (at r_1) and descends along the cold wall (at r_3). Thus, the liquid temperature at higher levels is greater than lower ones. The temperature difference between levels 1 and 3 will be smaller if the volume concentration increases; this occurs due to the enhancement of natural convection thermal characteristics inside the enclosure.

Figure 5a depicts time variations of the liquid mean temperature. In the initial stages, temperature rise of the liquids has the same rate. As time goes by, however, the rates deviate from each other depending on the fluid type. At the beginning, as the conduction layer thickness (Δ) is much smaller than the enclosure dimension (r_{31}) for water and nanofluids, e.g., $\Delta \approx 0.4$ mm at $t = 2$ min [36], a central region exists with a nearly uniform temperature; this region can therefore be modeled as isothermal. Following the conduction regime (i.e., at small Ra in which the velocities are small and essentially parallel to the surfaces), there is a transition period during which convection becomes established to a quasi-steady regime in which the bulk temperature of the liquid in the enclosure is gradually enhanced. With increasing Ra, the cellular flow intensifies and becomes concentrated in boundary layers adjoining the sidewalls. Estimation of the boundary layer thicknesses adjacent to the cylinders, e.g., $\delta \approx 43$ mm at height 0.1 m for water [37], reveals that the central region (which is stably stratified and almost stationary) disappears; boundary layers overlap and then occupy the annulus. This effect is certainly ensured by using nanofluids due to relatively smaller values of Rayleigh number; the typical values $Ra = 154,270$ for liquid B and $Ra = 244,925$ for liquid A are comparable [38–41]. To reach a specific temperature, liquid C needs the least time. This behavior coincides exactly with the time constant concept; any decrease in $c_{p,l}$ and/or in τ_t will cause the liquid to respond more rapidly to changes in its thermal environment. Time variations of average temperature of inner and outer walls are illustrated in Figs. 5b–d for water, 0.05% nanofluid, and 0.1% nanofluid, respectively. Time-averaged calculations display that $\Delta \bar{T}_{1-3} = \bar{T}(r_1) - \bar{T}(r_3)$ is 1.91, 2.18, and 2.22 °C for water, 0.05% nanofluid, and 0.1% nanofluid, respectively. It demonstrates that nanofluid with higher concentration will be relatively more efficient.

Figure 6 illustrates $\bar{h}_t$ for the liquids. It is observed that liquid C has a comparatively enhancement in the average convective heat transfer coefficient, especially at the second half of the heating process; since higher temperature of the base fluid results in more active Brownian motion of nanoparticles and consequently more effective thermal
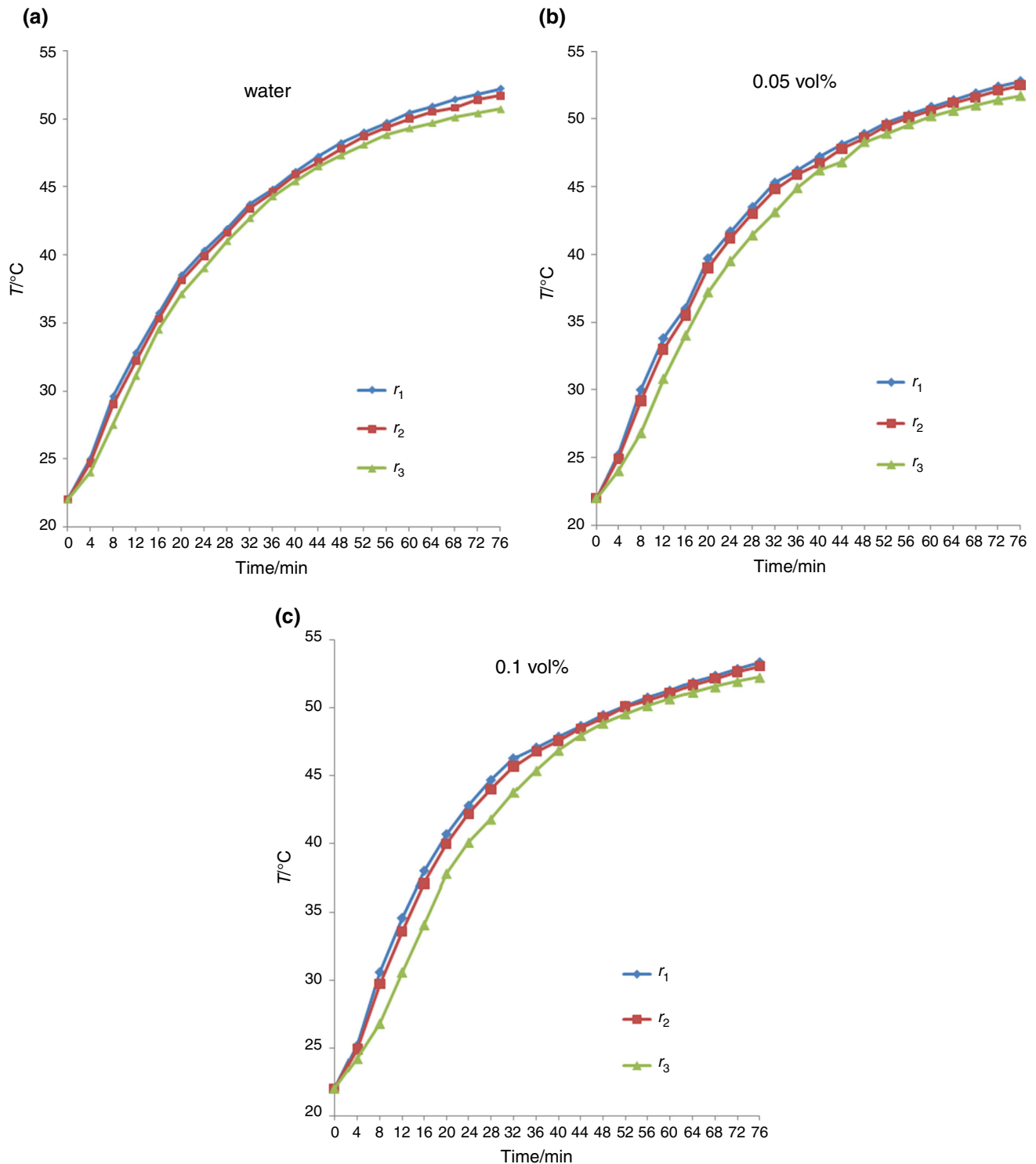
(a)

(b)

(c)

Fig. 3 Temperature variations with time at three different r values for a fixed $z = z_2$

conductivity. All the liquids experience a significant decline from the beginning (when $\bar{T}_s$ and $\bar{T}_m$ are almost equal and $\bar{h}_t$ is not normally defined) until the eighth minute, and then goes through a fluctuant upward trend. The quantity $\bar{h}_t$ exhibits very large values at the beginning of the process; the $\bar{h}_t$ values, for instance, at $t = 2$ min for liquids A, B, and C are 1366, 1549, and 1757 W m^{-2} K^{-1}, respectively. The biggest rise of $\bar{h}_t$ is reported for liquid C from the 30th min up to the 44th min standing at 740 W m^{-2} K^{-1}. Addition of Al$_2$O$_3$ nanoparticles into the

(a)

water

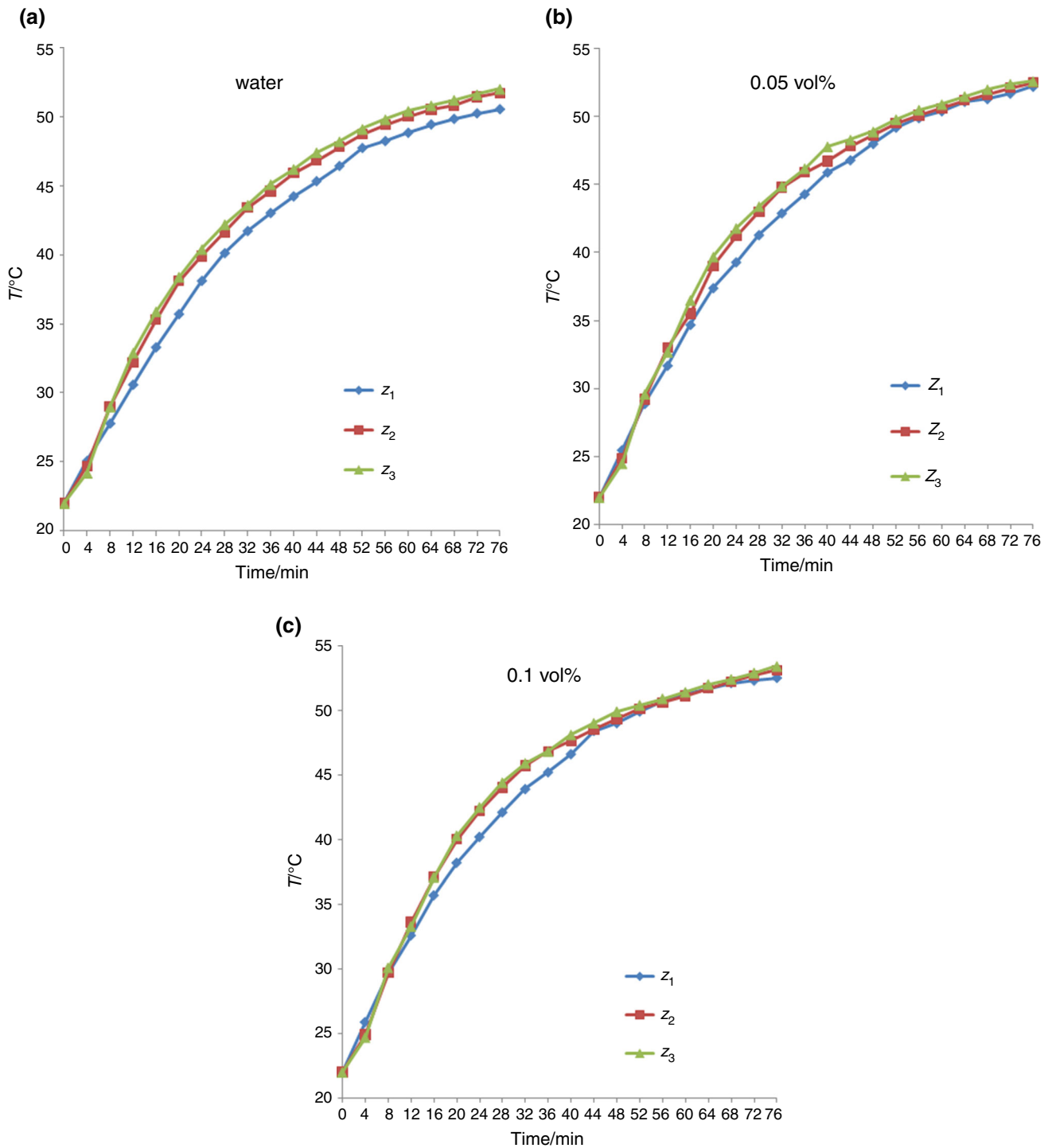(b)

0.05 vol%

(c)

0.1 vol%

Fig. 4 Temperature variations with time at three different z values for a fixed $r = r_2$

base fluid increases the effective convective coefficient and surface area.

In Fig. 7, the average heat flux of steel pipe for different working fluids is displayed. Heat flux is zero everywhere at the beginning; a start to the heating process makes the steel pipe (inner surface of the enclosure) warm, and so the surface temperature gradient is severely enhanced for a short time (e.g., the $\bar{q}_t''$ values for liquids A, B, and C approach approximately 199, 207, and 208 W m^{-2}, respectively, after 2 min); afterward a slight incline is observed. This upward trend continues until about the 30th min; then it drops slightly. Maximum average heat flux is
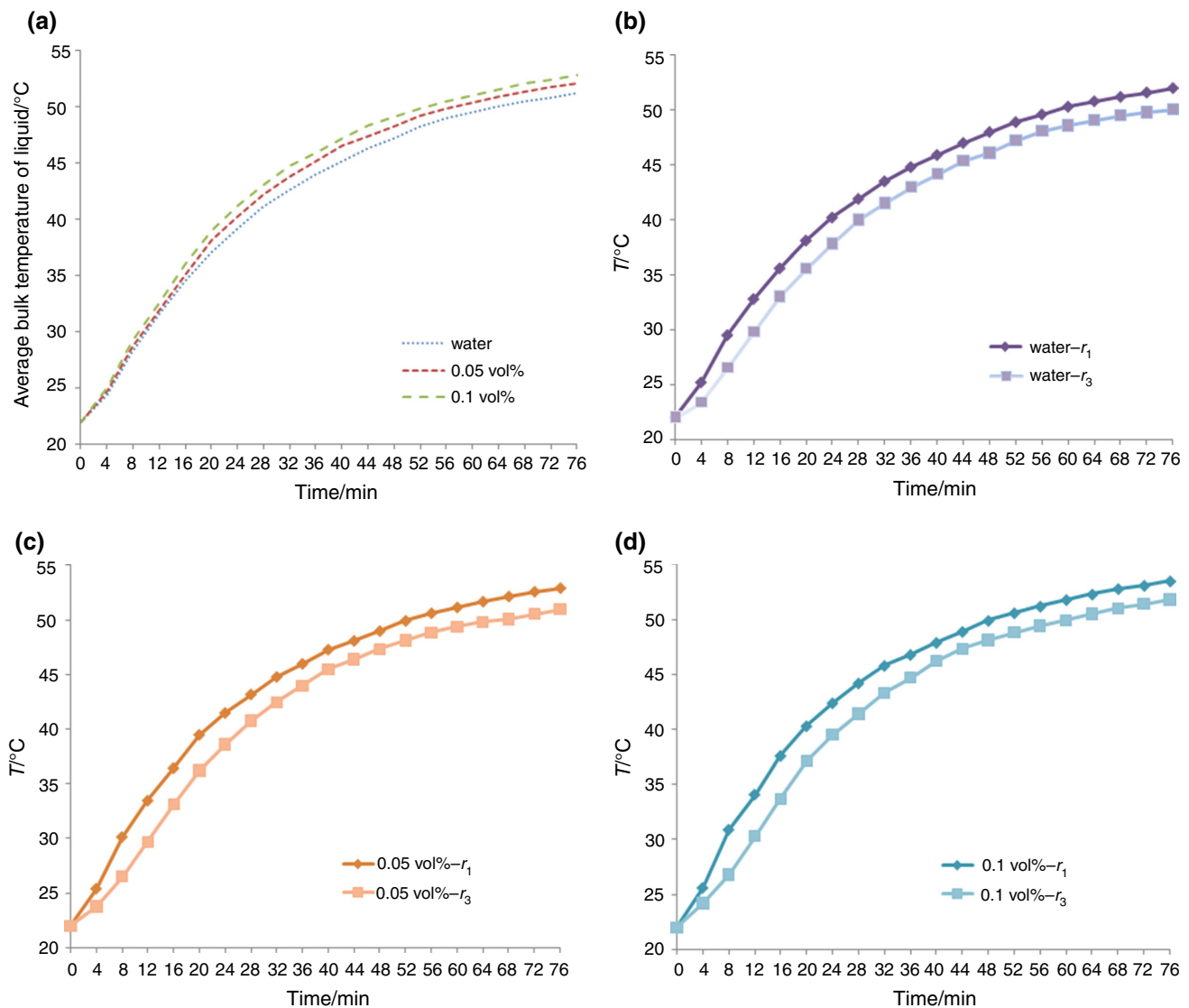
Fig. 5 **a** Variations of bulk fluid temperature with time for three various liquids; variations of average temperature at inner and outer walls for **b** water, **c** 0.05% nanofluid, and **d** 0.1% nanofluid

attained for liquid C (0.1% nanoparticle volume concentration) which is about 560 W m^{-2}. It is manifested that changes in the average heat flux corresponds with variations of the average heat transfer coefficient, the effective thermal conductivity, and the surface/bulk fluid temperature difference. $\bar{h}_t$ and k_{eff} are certainly improved with time, but $\Delta\bar{T}_{s-m}$ is normally diminished. The final outcome of these evidences confirm enhancement of the heat flux at the beginning of the process, a nearly flat rate at the middle stages, and a gradual decline at the rest of time. As liquid C exhibits higher heat flux values compared with the other liquids, it can gain more amount of heat.

Figure 8 shows the average Nusselt number for water, 0.05, and 0.1% volume concentrations. It is observed that all the working fluids experience a fluctuating upward

trend, then a gradually downward pattern. The decay of Nu in the later part of the process is insignificant for liquid C in contrast to the other liquids, since the thermal characteristics of the nanofluid are improved by increasing nanoparticles volume concentration, and thus the temperature difference between bulk fluid and surfaces is reduced. The average Nusselt number of liquid C is higher than the others, especially at the second half of the time interval (it has been measured about 86 at the highest point), which corresponds to higher values of $\bar{h}_t$. Very large Nu values are observed at the initial stages; e.g., 160, 181, and 208 at $t = 2$ min for liquids A, B, and C, respectively. A rapid decline in Nu is then observed until $t = 8$ min for all the liquids. It is stated that the average Nusselt number
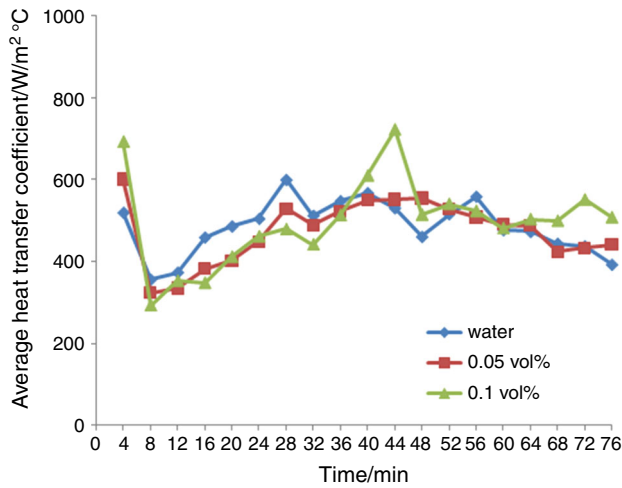
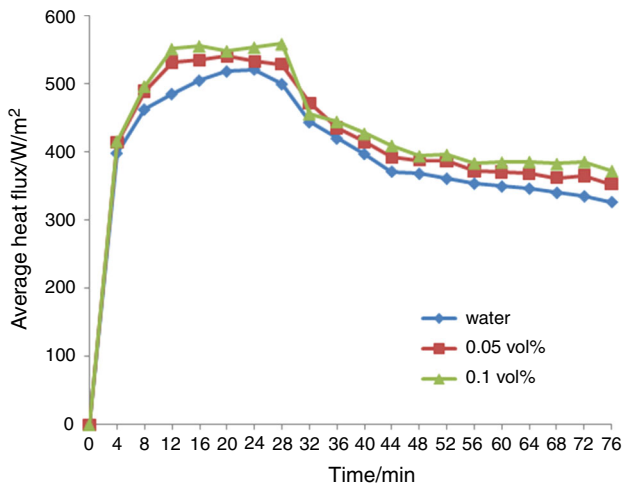**Fig. 6** Variations of $\bar{h}_t$ with time for three various liquids

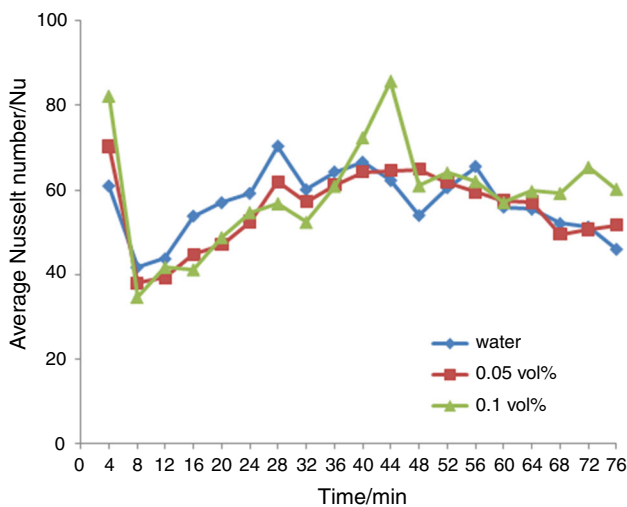**Fig. 7** Variations of $\bar{q}''_t$ with time for three various liquids

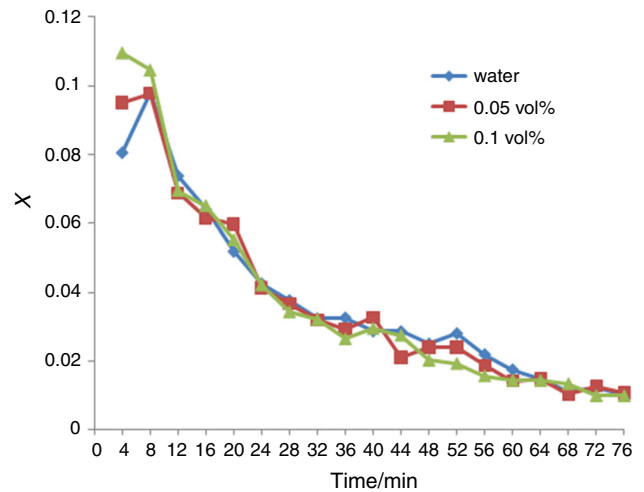**Fig. 8** Variations of Nu with time for three various liquids

Fig. 9 Temperature ratio versus time for three different fluids

increases with an increase in Al_2O_3 nanoparticle concentration in the base fluid.

In Fig. 9, the X dimensionless coefficient for the liquids is pointed out in the 4-min intervals. This quantity is the ratio of temperature rise in the liquid to the temperature difference in the gas (between levels z_1 and z_3). Ideally, the whole energy given to the liquid by the gas is absorbed by it (heat loss in the jacket is negligible). According to definition of ζ, however, the amount of average heat loss for liquids A, B, and C is 15.85, 14.96, and 15.69%, respectively. Hence, heat transferred by the exhaust gas to the working fluid is not completely applied to increase the temperature. It is evident that heat is partially dissipated by means of other components such as sensors, Teflon pipe (outer surface), gaskets. The temperature ratio (X) for the liquids decreases with time; since the ability of liquid in absorbing energy decreases with time, thus the difference in the average temperature of the liquid declines over the time span.

Concluding remarks

According to the comprehensive results, the following conclusions may be stated:

1. In the initial stages of the heating process, a high rate of the liquid temperature rise is observed. Asymptotic trends are then exhibited by water as well as nanofluids; the latter approaches a relatively higher temperature due to the enhanced thermal conductivity caused by the Brownian motion. For very small Rayleigh numbers, the liquid flow is sufficiently feeble that conduction is the only heat transfer mechanism.

2. As Ra is increased, a laminar boundary layer regime is established wherein the flow is largely restricted to the

boundary layers close to the cylinders. A circulating flow is generated for which liquid ascends along the hot wall and descends along the cold wall. Relative temperature uniformity will be ensured if the nanoparticles volume concentration increases to some degree.

3. Nanofluids with higher volume concentration need shorter time to reach a specific temperature (the more nanofluid has nanoparticle concentration, the shorter the response time to any changes in thermal surroundings will be).

4. Any increase in time constant will cause the liquid to respond more slowly to changes in its thermal immediate surroundings. This occurs practically whether the ratio of liquid/gas heat capacities is high or the gas mass flow rate is small.

5. Temperature difference between inner and outer surfaces of the enclosure increases with increasing nanoparticles volume concentration.

6. At the beginning of experiments, average convective heat transfer coefficient in the enclosure seems to be a large value; it is rapidly reduced for a particular time. Afterward it shows a fluctuating growing trend due to sequentially changes in effective thermal conductivity, surface temperature gradient, and surface/bulk fluid temperature difference. The convective heat transfer coefficient of liquid C becomes comparatively greater at the second half of the time interval due to higher temperature of the base fluid and consequently higher effective thermal conductivity.

7. Maximum heat flux at the inner wall is attained by nanofluids with higher volume concentration. As the experiment is in progress, the inner surface becomes hotter by the flue gas, while there is a delay in increasing the bulk fluid temperature; hence, the wall temperature gradient and consequently the heat flux are strongly enhanced to a certain time. Afterward a decline in the wall heat flux is ascertained, since the temperature difference between the wall and the bulk fluid is reduced due to the effects of circulating flows and natural convection phenomenon inside the enclosure. Meanwhile, as the nanofluid with higher concentration represents a comparatively higher wall heat flux at the whole time interval, it is relatively capable of absorbing more heat values.

8. Nusselt number decreases quickly first and then follows a fluctuating pattern. However, a maximum is reached at a particular time that depends on the volume fraction of nanoparticles in the base fluid.

9. Temperature ratio decreases with time due to reducing the ability of liquids to gain thermal energy.

10. By using 0.1% nanofluid, bulk fluid temperature, convective heat transfer coefficient, heat flux, and

Nusselt number are comparatively enhanced by 3.4, 20.58, 7.15, and 22.04%, respectively.

References

1. Choi S, Siginer DA, Wang HP. Enhancing thermal conductivity of fluids with nanoparticles in development and applications of non-newtonian flows. New York: ASME; 1995. p. 99–105.
2. Ghadimi A, Saidur R, Metselaar H. A review of nanofluid stability properties and characterization in stationary conditions. Int J Heat Mass Transf. 2011;54:4051–68.
3. Hwang Y, Lee JK, Lee JKU, Jeong Y, Cheong SI, Ahn YC, Kim SH. Production and dispersion stability of nanoparticles in nanofluids. Powder Technol. 2007;186:145–53.
4. Bejan A, Karaus AD. Heat transfer handbook. Hoboken: Wiely; 2003.
5. Choi SUS. Nanofluid technology: current status and future research. Vienna, VA, US: Korea-US. Technical Conference on Strategic Technologies; 1998.
6. Masuda H, Ebata A, Teramae K, Hishinuma N. Alteration of thermal conductivity and viscosity of liquid by dispersing ultrafine particles. Netsu Bussei. 1993;7:227–33.
7. Sridhara V, Satapathy LN. Al_2O_3-based nanofluids: a review. Nnoscale Res Lett. 2011;6(456):1–16.
8. Grimm A. Powdered aluminum-containing heat transfer fluids. German Patent DE 4131516A1; 1993.
9. Esfe MH, Saedodin S, Mahian O, Wongwises S. Thermal conductivity of Al_2O_3/water nanofluids. J Therm Anal Calorim. 2014;117:675–81.
10. Rashidi S, Mahian O, Languri EM. Applications of nanofluids in condensing and evaporating systems. J Therm Anal Calorim. 2018;131:2027–39.
11. Hung YH, Chen YH, Teng TP. Feasibility assessment of thermal management system for green power sources using nanofluid. J Nanomaterials. 2013; Article ID 321261: 11.
12. Amani M, Amani P, Kasaeian A, Mahian O, Wongwises S. Thermal conductivity measurement of spinel-type ferrite $MnFe_2O_4$ nanofluids in the presence of a uniform magnetic field. J Mol Liq. 2017;230:121–8.
13. Togun H, Abdulrazzaq T, Kazi SN, Badarudin A, Kadhum AAH, Sadeghinezhad E. A review of studies on forced, natural and mixed heat transfer to fluid and nanofluid flow in an annular passage. Renew Sustain Energy Rev. 2014;39:835–56.
14. Ravnik J, Škerget L. A numerical study of nanofluid natural convection in a cubic enclosure with a circular and an ellipsoidal cylinder. Int J Heat Mass Transf. 2015;89:596–605.
15. Amani M, Amani P, Kasaeian A, Mahian O, Pop I, Wongwises S. Modeling and optimization of thermal conductivity and viscosity of $MnFe_2O_4$ nanofluid under magnetic field using an ANN. Sci Rep. 2017;7:17369.
16. Arani AAA, Kakoli E, Hajialigol N. Double-diffusive natural convection of Al_2O_3–water nanofluid in an enclosure with partially active side walls using variable properties. J Mech Sci Technol. 2014;28:4681–91.
17. Abu-Nada E, Masoud Z, Oztop HF, Campo A. Effect of nanofluid variable properties on natural convection in enclosure. Int J Therm Sci. 2010;49:479–91.
18. Amani M, Amani P, Mahian O, Estelle P. Multi-objective optimization of thermophysical properties of eco-friendly organic nanofluids. J Clean Prod. 2017;166:350–9.
19. Esfe MH, Saedodin S, Mahian O, Wongwises S. Efficiency of ferromagnetic nanoparticles suspended in ethylene glycol for

applications in energy devices: effects of particle size, temperature, and concentration. Int Commun Heat Mass Transf. 2014;58:138–46.

20. Parizad RL, Rashidi S, Esfahani JA. Experimental investigation of nanofluid free convection over the vertical and horizontal flat plates with uniform heat flux by PIV. Adv Powder Technol. 2016;27:312–22.

21. Amani M, Ameri M, Kasaeian A. Hydrothermal assessment of ferrofluids in a metal foam tube under lowfrequency magnetic field. Int J Therm Sci. 2018;127:242–51.

22. Rashidi S, Eskandarian M, Mahian O, Poncet S. Combination of nanofluid and inserts for heat transfer enhancement: gaps and challenges. J Therm Anal Calorim. 2018. https://doi.org/10.1007/s10973-018-7070-9 (**Accepted**).

23. Moghadam AJ, Farzane-Gord M, Sajadi M, Hoseyn-zadeh M. Effects of CuO/water nanofluid on the efficiency of a flat-plate solar collector. Exp Thermal Fluid Sci. 2014;59:9–14.

24. Ghadiri M, Sardarabadi M, Pasandideh-fard M, Moghadam AJ. Experimental investigation of a PVT system performance using nano ferrofluids. Energy Convers Manag. 2015;103:468–76.

25. Moshizi SA, Malvandi A. Different modes of nanoparticle migration at mixed convection of Al_2O_3–water nanofluid inside a vertical microannulus in the presence of heat generation/absorption. J Therm Anal Calorim. 2016;126:1947–62.

26. Javadi P, Rashidi S, Esfahani JA. Flow and heat management around obstacle by nanofluid and incidence angle. J Thermophys Heat Transf. 2017;31:983–8.

27. Raei B, Shahraki F, Jamialahmadi M, Peyghambarzadeh SM. Experimental study on the heat transfer and flow properties of c-Al_2O_3/water nanofluid in a double-tube heat exchanger. J Therm Anal Calorim. 2017;127:2561–75.

28. Shirejini SZ, Rashidi S, Esfahani JA. Recovery of drop in heat transfer rate for a rotating system by nanofluids. J Mol Liq. 2016;220:961–9.

29. Shahriari A, Javaran EJ, Rahnama M. Effect of nanoparticles Brownian motion and uniform sinusoidal roughness elements on natural convection in an enclosure. J Therm Anal Calorim. 2018;131:2865–84.

30. Terhan M, Comakli K. Design and economic analysis of a flue gas condenser to recover latent heat from exhaust flue gas. Appl Thermal Eng. 2016;100:1007–15.

31. Shelke SA, Gohel NS. Heat transfer performance of a vertical thermosyphons heat pipe heat exchanger using hybrid nanofluid for automobile engine exhaust heat. Int J Curr Eng Technol. 2016;5:91–4.

32. Pak BC, Cho YI. Hydrodynamic and heat transfer study of dispersed fluids submicron metallic oxide particles. Exp Heat Transf Int. 1998;11:151–70.

33. Xuan Y, Roetzel W. Conception for heat transfer correlation of nanofluids. Int J Heat Mass Transf. 2000;43:3701–7.

34. Maxwell JC. A treatise on electricity and magnetism, vol. 1. Oxford: Clarendon; 1892.

35. Moffat R. Describing the uncertainties in experimental results. Exp Thermal Fluid Sci. 1988;1:3–17.

36. Rohsenow WM, Hartnett JP, Cho YI. Handbook of heat transfer. New York: McGraw-Hill; 1998.

37. Bergman TL, Lavine AS, Incropera FP, Dewitt DP. Fundamentals of heat and mass transfer. New York: Wiley; 2011.

38. Khanafer K, Vafai K, Lightstone M. Buoyancy-driven heat transfer enhancement in a two dimensional enclosure utilizing nanofluids. Int J Heat Mass Transf. 2003;46:3639–53.

39. Hwang KS, Lee JH, Jang SP. Buoyancy-driven heat transfer of water-based Al_2O_3 nanofluids in a rectangular cavity. Int J Heat Mass Transf. 2007;50:4003–10.

40. Ho CJ, Chen MW, Li ZW. Numerical simulation of natural convection of nanofluid in a square enclosure: effects due to uncertainties of viscosity and thermal conductivity. Int J Heat Mass Transf. 2008;51:4506–16.

41. Ho CJ, Liu WK, Chang YS, Lin CC. Natural convection heat transfer of alumina–water nanofluid in vertical square enclosures: an experimental study. Int J Thermal Sci. 2010;49:1345–53.